EAST EUROPEAN JOURNAL OF PHYSICS. 2. 281-286 (2025)
DOI:10.26565/2312-4334-2025-2-34 ISSN 2312-4334

PHOTODETECTORS FOR X- AND γ-RAY SCINTILLATORS

Mykola S. Kukurudziak*, Ivan P. Koziarskyi, Mykola S. Solodkyi, Eduard V. Maistruk[a], Vasylyna V. Kopach[a], Yurii O. Semeniuk[a], Mykola M. Pavliuk[a]
Yuriy Fedkovych Chernivtsi National University, Kotsyubyns'kogo str. 2, 58012, Chernivtsi, Ukraine
**Corresponding Author e-mail: mykola.kukurudzyak@gmail.com*
Received March 2, 2025; revised May 6, 2025 accepted May 13, 2025

The article analyzes X- and γ-ray detectors based on the ionizing and scintillation principles of operation. The effectiveness of using silicon *p-i-n* and *p-n* photodiodes in scintillation sensors for detecting visible photoluminescent radiation is investigated. The *p-i-n* detector was fabricated on the basis of *p*-type single crystal silicon with orientation [111] and resistivity 8-10 kΩ·cm. The *p-n* photodiode was fabricated on the basis of *n*-type single crystalline silicon with orientation [111] and resistivity 200-300 Ω·cm. It was found that *p-n* photodiodes have a much lower dark current than *p-i-n* photodiodes (although somewhat inferior in sensitivity), which provides their advantage in detectivity. However, if it is necessary to register short pulses of luminescent radiation, *p-i-n* photodiodes should be used, since they have a higher response speed. The increase in response speed is due to the fact that the process of diffusion of charge carriers in a *p-n* structure of a photodiode is replaced in the *p-i-n* structure by the drift of charge carriers through the *i*-region in a strong electric field.
Keywords: *Photoluminescence; Zinc Selenide; Silicon; CdTe; Electrical Properties; Detectivity; Photodiodes*
PACS: 61.72. Ji, 61.72. Lk, 85.60. Dw

Continuous scientific and technological progress will make it increasingly important to monitor and measure doses of ionizing radiation, in particular X-rays and γ-rays. These are high-energy types of radiation that can cause damage to cells and tissues of the body [1]. Therefore, controlling the level of these radiations is necessary to ensure the safety of people working in environments where these radiations may be present (e.g., medical facilities, nuclear power plants, industrial enterprises) [2]. Measurement of X-ray and gamma radiation levels is necessary to ensure the safe use of these methods in medical diagnostic procedures (radiography, computed tomography) and therapy (radiotherapy) [3]. When radioactive materials are used in industry, energy, or research, it is important to monitor the environment to detect and prevent radiation contamination in a timely manner. Measurements of X-rays and gamma rays are important in astrophysics, nuclear physics, and the study of cosmic phenomena, as these types of radiation are important indicators of various processes in the Universe, such as interaction with high energies.

Meeting these monitoring needs requires the development of new and improvement of existing approaches to the manufacture of ionizing radiation detectors. These approaches can be focused on improving sensitivity, accuracy, measurement speed, and ability to operate in difficult conditions.

The most common methods for detecting X- and γ-radiation that are being developed and improved are ionization and scintillation methods. The ionization method [4, 5] is based on measuring the ionization effect. It occurs in the sensitive volume of the detector when ionizing radiation interacts with it. Three types of ionization detectors are mainly used: a semiconductor detector, a pulsed ionization chamber with a grid, and a proportional counter [6]. However, semiconductor detectors are the most widely used. In a semiconductor detector, a sensitive region is created in which there are no free charge carriers. Once in this area, a charged particle causes ionization. Accordingly, holes appear in the valence band and electrons in the conduction band. Under the action of a voltage supplied to the electrodes deposited on the surface of the sensitive zone, the movement of holes and electrons occurs, which leads to the appearance of a current pulse. Devices for registering ionizing radiation are made both on the basis of elementary semiconductors and complex ones, including solid solutions. For example, spectrometers with silicon diffusion-drift detectors measure β-spectra, as well as X-ray and low-energy γ-ray spectra. Germanium detectors made it possible to create γ-spectrometers with high technical parameters. However, among the many complex semiconductors used for X- and γ-ray detectors at room temperature, such as halide perovskite semiconductors [7], thallium bromide [8], cadmium telluride-based detectors have been the most promising and studied compounds for many years [9-12]. At the same time, the most successful of the latter is CdZnTe [13-15]. However, due to the strict requirements for the properties of materials needed to operate at room temperature, they all have several critical problems. In particular, thallium bromide (TiBr) exhibits unresolved problems of contact deterioration and device polarization, although various solution approaches are being investigated [16]. The use of halide perovskite materials ($CsPbBr_3$) shows poor performance stability over time due to ion migration and defects under the influence of an electric field [17]. CdZnTe has some problems with Te inclusions, subgrain boundaries, and zinc segregation coefficient [18, 19]. Thus, the development of a nuclear detector based on a semiconductor that would have high performance and low cost at room temperature remains a significant challenge. An interesting fact is that the addition of impurities in the form of Mn

Cite as: M.S. Kukurudziak, I.P. Koziarskyi, M.S. Solodkyi, E.V. Maistruk, V.V. Kopach, Y.O. Semeniuk, M.M. Pavliuk, East Eur. J. Phys. 2, 281 (2025), https://doi.org/10.26565/2312-4334-2025-2-34

and Se results in the formation of solid solutions of the composition CdZnTeSe and CdMnTeSe, which exhibit improved electrophysical properties compared to CdTe [20, 21]. In particular, the addition of selenium leads to a sharp decrease in the density of dislocations and grain boundaries, and better compositional homogeneity [22]. The addition of manganese to CdTe can solve the problem of zinc segregation factor due to the more stable segregation property of manganese [23]. In [24], the suitability of CdMnTe and CdMnTeSe as materials for room temperature X-ray and γ-ray detectors was investigated and their crystal structures, mechanical and optical properties were studied.

However, the above are complex physical and technological problems that can be avoided by using scintillation detectors. These detectors use scintillation materials, materials that emit light when they absorb ionizing radiation. This light is converted into an electrical signal using photodiodes or photomultipliers [25].

The variety of scintillation materials is wide. For example, scintillation crystals based on ZnSe exhibit luminescence at λ = 460-590 nm when irradiated with X-rays [26, 27], scintillators based on polystyrene - λ = 425-530 nm [28, 29], bismuth germanate $Bi_4Ge_3O_{12}$ has a maximum luminescence at λ = 480 nm [30], yttrium aluminum garnet $Y_3Al_5O_{12}$: Ce (YAG:Ce), lutetium aluminum garnet ($Lu_3Al_5O_{12}$:Ce, LuAG:Ce), and yttrium lutetium aluminum garnet mixed crystals ($(Y,Lu)_3Al_5O_{12}$) have a scintillation wavelength of λ=530-550 nm, which is ideal for matching with photodiodes and avalanche photodiodes [31,32].

As can be seen from the above list of scintillation materials, detectors sensitive to the visible spectral range are required to detect their luminescent radiation. The development and improvement of these detectors is an urgent scientific and technical task. These can be avalanche photodiodes [33], photomultipliers [34], or *p-i-n* photodiodes [35,36], as well as *p-n* photodiodes [37]. The most widespread are scintillation detectors based on silicon *p-i-n* and *p-n* photodiodes.

The market leader in the production of silicon photodetectors is Humamatsu (Japan). The manufacturer offers a series of visible and near-infrared detectors for scintillators: S2744-08 [38], S2744-09 [39], S3204-08 [40], S3584-08 [41], S3590-18 [42] - *p-i-n* photodiodes of different areas are sensitive in the range of λ = 340-1100 nm with a maximum at λ = 960 nm and photosensitivity S = 0.2-0. 4 A/W in the visible range; as well as S12497 [43] and S12498 [44] - *p-n* photodiodes are sensitive in the range of λ = 400-1100 nm with a maximum at λ = 920 nm and a photosensitivity of S = 0.32-0.36 A/W at λ = 540 nm.

As can be seen from the analysis of the detectors, their spectral maximum is shifted towards the near-infrared region, respectively, shifting the maximum towards shorter wavelengths may increase the sensitivity of the detectors in a given range. No less urgent is the need to reduce the dark currents of the detectors to ensure their significant detectivity. Accordingly, the aim of this work is to develop silicon *p-i-n* and *p-n* photodiodes for the visible range, to characterize them comparatively and to study the possibilities of increasing their detectivity and reducing the dark current (I_d) for effective use in scintillation detectors.

EXPERIMENTAL

Two types of single-element PDs of the same area, *p-i-n* and *p-n*, were fabricated for the detection of photoluminescent radiation in the visible range. The *p-i-n* detector was fabricated on the basis of *p*-type single crystal silicon with orientation [111] and resistivity ρ≈8-10 kΩ·cm according to the technical regimes given in [45]. The structure of the PD crystal with a guard ring (GR) was used to prevent the influence of inversion layers at the Si-SiO_2 interface on the parameters of the PD and surface breakdown (Fig. 1a). The n^+-type responsive element (RE) and GR were formed by phosphorus diffusion. The depth of the phosphorus impurity reached x_{n+-p}=2-2.5 μm. The p^+-type ohmic contact on the reverse side of the crystal was formed by boron diffusion. The antireflective SiO_2 on the surface of the RE was formed by oxidation in a dry oxygen atmosphere and met the condition of minimum reflection [46]:

$$\frac{\lambda}{4} = n d_{SiO2} \tag{1}$$

where λ is the working wavelength; n the refractive index of SiO_2; d_{SiO2} is the thickness of the antireflective film.

Considering that the fabricated PDs are planned to be used for detecting wavelengths in the range of λ = 400-780 nm, in which the thickness of the antireflection oxide reaches d_{SiO2} = 70-140 nm, we formed an intermediate thickness of the oxide film d_{SiO2} = 100-110 nm.

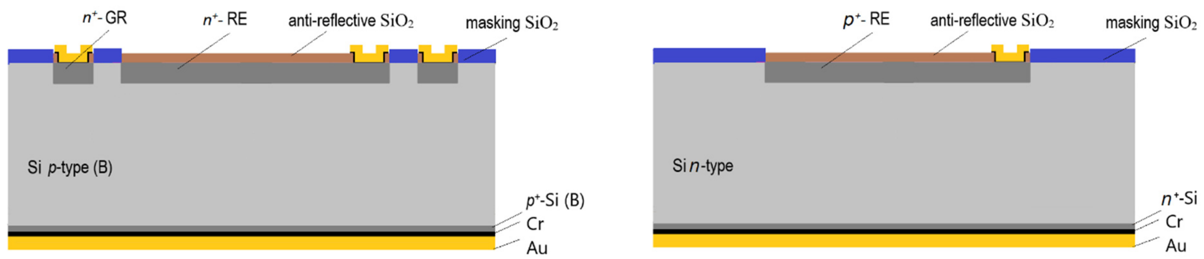

a) b)

Figure 1. Schematic cross-section of *p-i-n* PD (a) and *p-n* PD (b)

The *p-n* PD was fabricated on the basis of *n*-type single crystalline silicon with orientation [111] and resistivity ρ≈200-300 Ω·cm (Fig. 1b). The topology without GR was used. The p^+-type RE was formed by boron diffusion (x_{p+-p}=2-2.5 μm). The n^+-type ohmic contact on the back side of the crystal was formed by phosphorus diffusion.

The parameters of the obtained PDs were compared.

RESULTS OF THE RESEARCH AND THEIR DISCUSSION

From the dark *I-V*-characteristics of the studied samples, it can be seen (Fig. 2) that the *p-n* PD has a significantly lower dark current than the *p-i-n* PD. This can be explained by considering the components of the dark current. The dark current of the PD is determined by the sum of the diffusion current in the neutral region (I_{dif}) (1) and the generation current in the depleted region (I_G) (2) [47].

$$I_{dif} = e\left(n_p \cdot \sqrt{\frac{D_n}{\tau_n}} + p_n \cdot \sqrt{\frac{D_p}{\tau_p}}\right) \quad (2)$$

where e is the electron charge, n_p and p_n are the concentrations of electrons and holes in the *p*- and *n*-layers, respectively, D_n and D_p are the diffusion coefficients of electrons and holes, respectively, τ_p and τ_n are the lifetimes of electrons and holes as minor charge carriers, respectively.

$$I_G = \mathrm{e}\frac{n_i}{2\tau} W_i A_{\mathrm{RE}} \quad (3)$$

where n_i is intrinsic concentration of charge carriers in the substrate; W_i is width of the space charge region, A_{RE} is the area of RE, τ is the effective lifetime of minor charge carriers.

The main contribution to the value of the PD dark current is made by the generation component, which is proportional to the width of the spatial charge region (SCR), which in turn is directly proportional to the reverse bias voltage [48]:

$$W_i = \left(\frac{2\varepsilon\varepsilon_0\,(\phi_c - U_{bias})}{eN_A}\right)^{\frac{1}{2}} \quad (4)$$

where ε, ε_0 are dielectric constants for silicon and vacuum, respectively; φ_c is contact potential difference.

If we calculate W_i for *p-i-n* PD and *p-n* PD, for example, at $|10\ \mathrm{V}|$, we obtain W_i = 95-105 μm in *p-i-n* PD and W_i = 15-20 μm in *p-n* PD. Accordingly, the generation dark current of *p-i-n* PD is much higher than that of *p-n* PD. Also, we note that the dependence of the dark current on the voltage in the *p-i-n* structure is stronger.

It is worth noting that in the case of manufacturing *p*-Si-based PDs (especially high-resistance ones), a surface component of the dark current (I_d^{surf}) is added (5), which characterizes the generation of charge carriers on the silicon-silicon oxide interface and in the region of the *p-n* junction exit to the crystal surface. It is the GR that is the element of the PD crystal that limits the surface component of the dark current, since in the presence of inversion layers at the Si-SiO_2 interface, the *p-n* junction area increases, and, accordingly, I_d increases (Fig. 2 inset) [49].

$$\mathrm{I}_d^{surf.} = \frac{\mathrm{e}N_{ss}v\sigma_{ss}A_{p-n}}{2} \quad (5)$$

where σ_{ss} is the cross section of the capture, N_{ss} is the density of surface states, v – is the average relative velocity of thermal charge carriers, A_{p-n} is the area of the *p-n* junction.

The use of the GR in the design of the PD crystal requires control of the insulation resistance between the GR and the RE [49]. In the investigated case, it reached about 1-2 MΩ.

The light *I-V*-characteristic of the PDs at λ = 405 nm, λ = 646 nm, λ = 780 nm (Fig. 3) were obtained and their sensitivity (*S*) was determined by formula (6) [50].

$$S = \left(I_{ph} - I_d\right)/P_{opt} \quad (6)$$

where I_{ph} is the light current of the PD, P_{opt} is the power of the radiation.

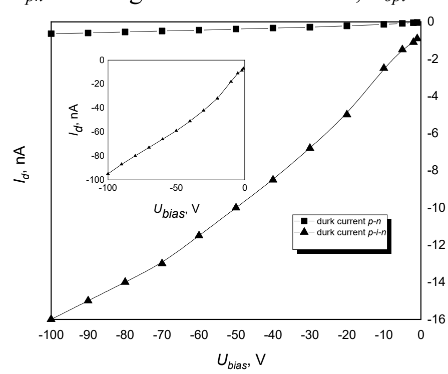

Figure 2. Reverse dark *I–V*-characteristics of PDs (insert is the dark *I–V*-characteristics of *p-i-n* PD without the connected GR)

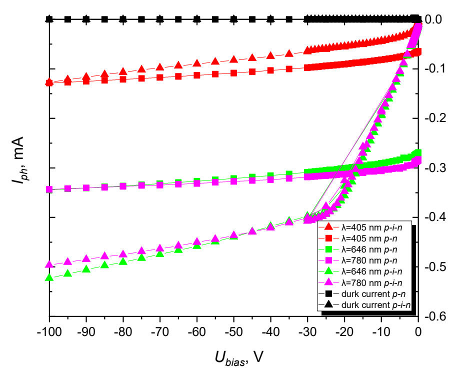

Figure 3. Reverse light *I–V*-characteristics of PDs (P_{opt}=5 mW)

In both cases, with an increase in the radiation wavelength, the photocurrent and sensitivity of the PDs increased, since the maximum of their spectral characteristics was shifted to longer wavelengths.

The absorption coefficient of the wave λ = 405 nm in silicon is $\alpha = 10^5$ cm^{-1} [51], respectively, the intensity of radiation with this wavelength, according to the Bouguer-Lambert-Beer law [52], decreases by a factor of *e* in the thickness of silicon about 1 μm (we assume that it is absorbed). Accordingly, in both studied samples, this radiation is absorbed in the doped layer, so the expansion of the SCR does not affect the collection of photogenerated charge carriers. Photogenerated charge carriers, in the described case, reach the *p-n* junction by diffusion due to the concentration gradient.

From the light *I-V*-characteristics of the PDs and the dependence of $S(U_{bias})$ (Fig. 4) at λ = 646 nm, λ = 780 nm, it is clear that the photocurrent and sensitivity of the *p-n* PD depend on the reverse voltage applied minimally, since its SCR changes minimally when the voltage is changed due to the low resistivity of the base material. It is known [53] that the *p-n* junction is reached only by those charge carriers that are photogenerated at a distance of the sum of the SCR width and the diffusion length of minor charge carriers from the *p-n* junction. Given that the SCR in this case changes minimally, and the diffusion length of the charge carriers is constant, the increase in photosensitivity with an increase in the reverse voltage is minimal.

In the case of *p-i-n* PDs, a slightly higher value of the photocurrent and sensitivity and a stronger dependence on voltage (at λ = 646 nm, λ = 780 nm) were observed due to an increase in W_i. At a reverse bias of 20-25 V, the photosensitivity of the PD reaches quasi-saturation, which indicates the complete collection of photogenerated charge carriers at this voltage.

In order to evaluate the photodetectors, their detectivity (D^*) was quantified using formula (7) [50], and the dependence $D^*(U_{bias})$ was obtained (Fig. 5).

$$D^* = \sqrt{\frac{A_{RE}}{2eI_d}}S \tag{7}$$

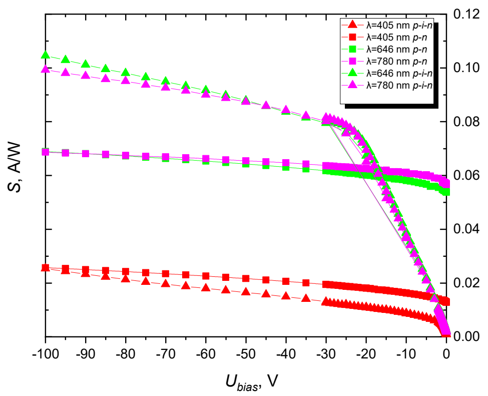

Figure 4. Dependence of the $S(U_{bias})$ of PDs

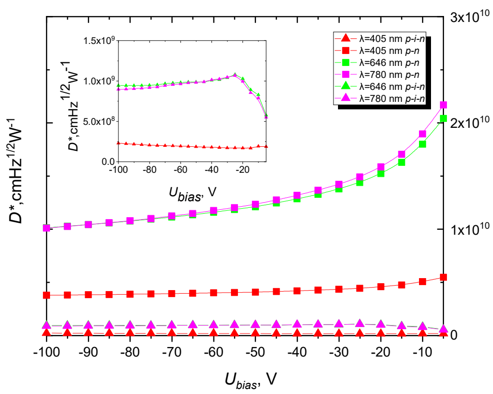

Figure 5. Dependence of the $D^*(U_{bias})$ of PDs (insert dependence of the $D^*(U_{bias})$ of *p-i-n* PD)

As can be seen from Fig. 5, *p-n* PD have much higher detectivity than *p-i-n* PD due to much lower dark currents, and thus this class of PD can be effectively used in scintillators where there is a need to detect weak optical signals. However, it should be noted that sometimes there is a need to register short pulses of photoluminescent radiation [54], in which case *p-i-n* PDs, although inferior in detectivity, are superior in response speed. The increase in speed is due to the fact that the process of diffusion of charge carriers in a conventional *p-n* structure of a photodiode is replaced in the *p-i-n* structure by the drift of carriers through the *i*-region in a strong electric field [55]. The drift time of electrons t_{dr} through the *i*-region with a width W_i and electric field intensity E is [48]:

$$t_{dr} = \frac{W_i}{v_n} = \frac{W_i}{\mu_n E} \tag{8}$$

were $v_n = \mu_n E$ is the speed of electron drift in an electric field, μ_n is the mobility of electrons.

The ratio of the electron drift time through the *i*-region to the diffusion time through the base of the *p-n* PD (t_{dif}) can be represented as:

$$\frac{t_{dr}}{t_{dif}} = \frac{W_i/\mu_n E}{W_i^2/2D_n} = \frac{W_i^2/\mu_n U_{bias}}{W_i^2/2D_n} = \frac{2\varphi}{U_{bias}} \tag{9}$$

Since $D_n/\mu_n = kT/q = \varphi$, where k is the Boltzmann constant and T is the temperature.

CONCLUSIONS

The analysis of ionizing radiation detectors based on semiconductor structures and scintillators is carried out. It is possible to avoid the technological difficulties of obtaining perfect semiconductor detectors based on CdTe compounds by using scintillators. The possibilities of using silicon *p-i-n* and *p-n* photodiodes to register the visible luminescent radiation of scintillation detectors are investigated. It was found that the *p-n* photodiodes have a significantly lower dark current than *p-i-n* photodiodes (by about an order of magnitude), which ensures their higher detectivity. However, *p-i-n* photodiodes have an advantage in response speed.

Acknowledgments

This work was partially supported by Ministry of Education and Science of Ukraine (grant number 0125U000832, authors M.S. Kukurudziak and M.S. Solodkyi, V.V. Kopach).

ORCID

Mykola S. Kukurudziak, https://orcid.org/0000-0002-0059-1387; **Ivan P. Koziarskyi,** https://orcid.org/0000-0002-4984-4349
Mykola S. Solodkyi, https://orcid.org/0000-0001-7432-9202; **Eduard V. Maistruk**, https://orcid.org/0000-0002-9025-6485
Vasylyna V. Kopach, https://orcid.org/0009-0004-7927-983X; **Yurii O. Semeniuk,** https://orcid.org/0009-0003-4900-7334
Mykola M. Pavliuk, https://orcid.org/0009-0008-4578-7288

REFERENCES

[1] T.B. Feldman, M.A. Yakovleva, and M.A. Ostrovsky, Experimental Eye Research, **252**, 110270 (2025). https://doi.org/10.1016/j.exer.2025.110270
[2] B. Huang, Y. Liu, X. Sun, L. Huang, S. Dong, and L. Mao, National Science Open, **4**(1), 20240021 (2025). https://doi.org/10.1360/nso/20240021
[3] D.P. Frush, et al., Journal of Applied Clinical Medical Physics, **e70022**, 1-11 (2025). https://doi.org/10.1002/acm2.70022
[4] N. Tsoulfanidis, and S. Landsberger, Measurement and Detection of Radiation (CRC Press, 2021). https://doi.org/10.1201/9781003009849
[5] Y. He, I. Hadar, and M.G. Kanatzidis, Nature Photonics, **16**(1), 14-26 (2022). https://doi.org/10.1038/s41566-021-00909-5
[6] R.V. Berestov, and N.Ye. Hots, Visnyk Cherkaskoho derzhavnoho tekhnolohichnoho universytetu. Tekhnichni nauky, **3**, 14-23 (2021). https://doi.org/10.24025/2306-4412.3.2021.243580 (in Ukrainian)
[7] Y. He, et al., Nature Photonics, **15**, 36–42 (2021). https://doi.org/10.1038/s41566-020-00727-1
[8] A. Datta, et al., Applied Physics Letters Materials, **5,** 106109 (2017). https://doi.org/10.1063/1.5001181
[9] N. Vyhnan, and Y. Khalavka, Luminescence, **29**(7), 952-954 (2014). https://doi.org/10.1002/bio.2600
[10] I. Fodchuk, et al., Proceedings of SPIE, **11369**, 113691H (2020). https://doi.org/10.1117/12.2553970
[11] D. Vorontsov, et al., CrystEngComm, **19**(45), 6804–6810 (2017). https://doi.org/10.1039/C7CE01688C
[12] I. Fodchuk, et al., Physics and Chemistry of Solid State, **23**(1), 144-149 (2022). https://doi.org/10.15330/pcss.23.1.144-149
[13] E.V. Maistruk, et al., Engineering Research Express, **2**(3), 035037 (2020). https://doi.org/10.1088/2631-8695/abb7e5
[14] E.V. Maistruk, et al., Journal of Nano- and Electronic Physics, **11**(2), 02007 (2019). https://doi.org/10.21272/jnep.11(2).02007
[15] I.G. Orletskyi, et al., Materials Research Express, **8**(1), 015905 (2021). https://doi.org/10.1088/2053-1591/abdbf8
[16] K. Takagi, et al., in: IEEE Transactions on Nuclear Science, **68**(9), 2435–2439 (2021). https://doi.org/10.1109/TNS.2021.3078448
[17] B.B. Zhang, et al., Applied Physics Letters, **116**, 063505 (2020). https://doi.org/10.1063/1.5134108
[18] A.E. Bolotnikov, et al., in: 2007 IEEE *Nuclear Science Symposium Conference Record*, 1788-1797, (2007). https://doi.org/10.1109/NSSMIC.2007.4436507
[19] A.E. Bolotnikov, et al., Journal of Crystal Growth, **379**, 46-56 (2013). https://doi.org/10.1016/j.jcrysgro.2013.01.048
[20] O. Kopach, et al., Journal of Phase Equilibria and Diffusion, **45**, 612-620 (2024). https://doi.org/10.1007/s11669-024-01116-9
[21] V. Kopach, et al., in: Proc. SPIE. Hard X-Ray, Gamma-Ray, and Neutron Detector Physics XXIII, **11838**, 1183819, 155–161 (2021). https://doi.org/10.1117/12.2594545
[22] U.N. Roy, et al., Sci. Rep. **9**, 7303 (2019). https://doi.org/10.1038/s41598-019-43778-3
[23] S.U. Egarievwe et al. "Advances in CdMnTe Nuclear Radiation Detectors Development", IEEE Nuclear Science Symposium and Medical Imaging Conference Proceedings (NSS/MIC), Sydney, NSW, Australia, pp. 1-3 (2018).
[24] A. Masłowska, et al., Sensors, **24**(2), 345 (2024). https://doi.org/10.3390/s24020345
[25] W.W. Moses, Nuclear Instruments and Methods in Physics Research Section A: Accelerators, Spectrometers, Detectors and Associated Equipment, ***487***(1-2), 123-128 (2002). https://doi.org/10.1016/S0168-9002(02)00955-5
[26] M.A. Jafarov, and S. A. Jahangirova, Phys. Solid State, **67**, 207–213 (2025). https://doi.org/10.1134/S106378342460211X
[27] O.H. Trubayeva, et al., Tekhnologiya i Konstruirovanie v Elektronnoi Apparature, **3**, 43-49 (2018). http://dx.doi.org/10.15222/TKEA2018.3.43 (in Ukrainian)
[28] S. Bhatnagar, arXiv preprint arXiv:2401.14706 (2024). https://doi.org/10.48550/arXiv.2401.14706
[29] Y.L. Yan, et al., J. Polym. Res., **32**, 19 (2025). https://doi.org/10.1007/s10965-024-04206-x
[30] I.L. Matos, et al.,Int. J. Appl. Ceram. Technol., **22**(1), e14911 (2025). https://doi.org/10.1111/ijac.14911
[31] P. Roos, in: *Handbook of Nuclear Medicine and Molecular Imaging for Physicists* (ed. by M. Ljungberg) (CRC Press, 107-128, 2022). https://doi.org/10.1201/9780429489556.
[32] N. Cichocka, et al., Nanotechnology, **33**(3),035702 (2021). https://doi.org/10.1088/1361-6528/ac2e74
[33] J. Jegal, H.W. Park, and H.J. Kim, IEEE Transactions on Nuclear Science, **68**(6), 1304-1308 (2021) https://doi.org/10.1109/TNS.2021.3070040
[34] S.J. van der Sar, S.E. Brunner, and D.R. Schaart, Medical Physics, **48**(10), 6324-6338 (2021). https://doi.org/10.1002/mp.14886
[35] M.S. Kukurudziak, and E.V. Maistruk, in: *Fifteenth International Conference on Correlation Optics*, 121261V (SPIE, Chernivtsi, 2021). https://doi.org/10.1117/12.2616170
[36] S.A. Canazza, et al., in: 2021 International Nuclear Atlantic Conference – INAC 2021 Virtual meeting, (2021). http://repositorio.ipen.br/handle/123456789/32524
[37] Z.W. Bell, Scintillators and Scintillation Detectors. in: Handbook of Particle Detection and Imaging, (Springer, Cham. 413-449, 2021). https://doi.org/10.1007/978-3-319-93785-4_15

[38] Passport data Si PIN photodiodes S2744/S3588-08, -09, Electronic resource https://www.hamamatsu.com/content/dam/hamamatsu-photonics/sites/documents/99_SALES_LIBRARY/ssd/s2744-08_etc_kpin1049e.pdf)
[39] Passport data Si PIN photodiodes S2744-09, https://www.hamamatsu.com/jp/en/product/optical-sensors/photodiodes/si-photodiodes/S2744-09.html
[40] Passport data Si PIN photodiode S3204-08, https://www.hamamatsu.com/jp/en/product/optical-sensors/photodiodes/si-photodiodes/S3204-08.html
[41] Passport data Si PIN photodiodeS3584-08, https://www.hamamatsu.com/jp/en/product/optical-sensors/photodiodes/si-photodiodes/S3584-08.html
[42] Passport data Si PIN photodiode S3590-18, https://www.hamamatsu.com/jp/en/product/optical-sensors/photodiodes/si-photodiodes/S3590-18.html
[43] Passport data Si photodiode S12497, https://www.hamamatsu.com/jp/en/product/optical-sensors/photodiodes/si-photodiodes/S12497.html
[44] Passport data Si photodiode S12498, https://www.hamamatsu.com/jp/en/product/optical-sensors/photodiodes/si-photodiodes/S12498.html
[45] M.S. Kukurudziak, Journal of nano- and electronic physics, **14**(1), 01023 (2022). https://doi.org/10.21272/jnep.14(1).01023
[46] S.B. Khan, S. Irfan, Z. Zhuanghao and S.L. Lee, Materials, **12**(9), 1483 (2019). https://doi.org/10.3390/ma12091483
[47] K.V. Ravi, *Imperfections and impurities in semiconductor silicon*, (Wiley, New York, 1981).
[48] N.M. Tugov, B.A. Glebov, and N. Charykov, *Semiconductor devices: Textbook for universities*, edited by V.A. Labuntsov, (Energoatomizdat, Moscow, 1990). (in Russian)
[49] M.S. Kukurudziak, Journal of Instrumentation, **19**(09), P09006 (2024). https://doi.org/10.1088/1748-0221/19/09/P09006
[50] S.N. Moger, and M. Mahesha, Sensors and Actuators A: Physical, **315**, 112294 (2020). https://doi.org/10.1016/j.sna.2020.112294
[51] S.M. Sze, and K.K. Ng, *Physics of semiconductor devices*, (Wiley, 2006).
[52] A.V. Igo, Opt. Spectrosc. **128**, 1125 (2020). https://doi.org/10.1134/S0030400X20080135
[53] M.S. Kukurudziak, and E.V. Maistruk, East Eur. J. Phys. **1**, 386 (2024). https://doi.org/10.26565/2312-4334-2024-1-39
[54] J.J. van Blaaderen, *et. al*., Chemistry of Materials, **37**(5), 1716-1740 (2025) https://doi.org/10.1021/acs.chemmater.4c03437
[55] A. Rawat, and M.S. Islam, in: *Physics and Simulation of Optoelectronic Devices* XXXII. SPIE, 12880, 128800Q (2024). https://doi.org/10.1117/12.3003413

ФОТОПРИЙМАЧІ ДЛЯ СЦИНТИЛЯТОРІВ РЕНТГЕНІВСЬКОГО ТА γ-ВИПРОМІНЮВАННЯ†

Микола С. Кукурудзяк, Іван П. Козярський, Микола С. Солодкий, Едуард В. Майструк, Василина В. Копач, Юрій О. Семенюк, Микола М. Павлюк
Чернівецький національний університет імені Юрія Федьковича, 58002, м. Чернівці, вул. Коцюбинського, 2, Україна

У статті проаналізовано детектори рентгенівського та γ-випромінювання на основі іонізаційного та сцинтиляційного принципів дії. Досліджено ефективність використання кремнієвих *p-i-n* і *p-n* фотодіодів у сцинтиляційних сенсорах для детектування видимого фотолюмінесцентного випромінювання. Детектор на основі *p-i-n*-структури виготовлено на основі монокристалічного кремнію *p*-типу з орієнтацією [111] та питомим опором 8-10 кОм·см. Фотодіод на основі *p-n*-структури виготовлявся на основі монокристалічного кремнію *n*-типу з орієнтацією [111] та питомим опором 200-300 Ом·см. Встановлено, що *p-n* фотодіоди мають значно менший темновий струм, ніж *p-i-n* фотодіоди (хоча дещо поступаються за чутливістю), що забезпечує їх перевагу в детективності. Однак, якщо необхідно реєструвати короткі імпульси люмінесцентного випромінювання, слід використовувати *p-i-n* фотодіоди, оскільки вони мають вищу швидкодію. Збільшення швидкості відгуку пов'язано з тим, що процес дифузії носіїв заряду в *p-n* структурі фотодіода замінюється в *p-i-n* структурі дрейфом носіїв заряду через *i*-область в сильному електричному полі.

Ключові слова: *фотолюмінесценція; селенід цинку; кремній; CdTe; електричні властивості; детектування; фотодіоди*